Thermal Unfolding of Triosephosphate Isomerase from *Entamoeba histolytica*: Dimer Dissociation Leads to Extensive Unfolding[†]

Luis A. Tellez,[‡] Luis M. Blancas-Mejia,[‡] Ernesto Carrillo-Nava,[§,||] Guillermo Mendoza-Hernández,[‡] David A. Cisneros,[‡,⊥] and D. Alejandro Fernández-Velasco*,[‡]

Laboratorio de Fisicoquímica e Ingeniería de Proteínas, Departamento de Bioquímica, Facultad de Medicina, and Departamento de Fisicoquímica, Facultad de Química, Universidad Nacional Autónoma de México, Apdo. Postal 70-159, 04510 México, DF

Received July 19, 2008; Revised Manuscript Received September 4, 2008

ABSTRACT: In mesophiles, triosephosphate isomerase (TIM) is an obligated homodimer. We have previously shown that monomeric folding intermediates are common in the chemical unfolding of TIM, where dissociation provides 75% of the overall conformational stability of the dimer. However, analysis of the crystallographic structure shows that, during unfolding, intermonomeric contacts contribute to only 5% of the overall increase in accessible surface area. In this work several methodologies were used to characterize the thermal dissociation and unfolding of the TIM from *Entamoeba histolytica* (EhTIM) and a monomeric variant obtained by chemical derivatization (mEhTIM). During EhTIM unfolding, sequential transitions corresponding to dimer dissociation into a compact monomeric intermediate followed by unfolding and further aggregation of the intermediate occurred. In the case of mEhTIM, a single transition, analogous to the second transition of EhTIM, was observed. Calorimetric, spectroscopic, hydrodynamic, and functional evidence shows that dimer dissociation is not restricted to localized interface reorganization. Dissociation represents 55% ($\Delta H_{Diss} = 146.8$ kcal mol^{-1}) of the total enthalpy change ($\Delta H_{Tot} = 266$ kcal mol^{-1}), indicating that this process is linked to substantial unfolding. We propose that, rather than a rigid body process, subunit assembly is best represented by a fly-casting mechanism. In TIM, catalysis is restricted to the dimer; therefore, the interface can be viewed as the final nucleation motif that directs assembly, folding, and function.

Triosephosphate isomerase (E.C. 5.3.1.1) (TIM) is a key glycolytic enzyme. In mesophiles, TIM is an obligated dimer made of identical subunits folded into $(\beta/\alpha)_8$ barrels (*1*). The three-dimensional structures and catalytic properties of TIM from different species are quite similar (*2, 3*). In contrast, the folding pathway of TIM from different organisms is rather diverse. Unfolding transitions have been described by models which increase in complexity from equilibrium (*4*−*6*) to kinetically controlled unfolding (*7*) and from two-state to multistate reactions that involve monomeric and/or dimeric intermediates (*5, 8*−*17*). The most common intermediates are monomers, which have been observed when the protein is chemically unfolded. Analysis of the crystallographic structure of TIM shows that, in the transition from the native dimer to the unfolded monomers, intermonomeric contacts account for ∼5% of the overall increase in accessible surface area. Nevertheless, the characterization of TIM unfolding from several organisms shows that the dissociation step accounts for ∼75% of the overall conformational stability of the dimer (*9, 10*). The reasons for this behavior are not fully understood because the conformational and thermodynamic consequences of dissociation have not been described in detail. Monomeric intermediates from several sources observed in TIM unfolding induced by Gdn-HCl have been studied. For example, pulse-field gradient NMR measurements suggested a compact intermediate ($R_s = 24$ Å) for TIM from *Saccharomyces cerevisiae* (ScTIM)[1] (*12*). On the other hand, the Stokes radii obtained by size exclusion chromatography for the intermediate and the native dimer are indistinguishable ($R_s = 30$ Å) (*10*). Similar expanded

[†] This work was partially supported by CONACYT grants (43592, 41328, and 61044-M), PAPIIT (IN218707-2), and Junta de Andalucía and UAM Acuerdos 11 and 13/07 del Rector General. Part of this work was performed by D.A.F.-V. during a sabbatical stay at the Departamento de Ciencias Naturales and the Departamento de Química, Universidad Autónoma Metropolitana, México, and the Departamento de Química Física, Facultad de Ciencias, Universidad de Granada, España.

* To whom correspondence should be addressed. E-mail: fdaniel@servidor.unam.mx. Telephone: (5255) 56232259. Fax: (5255) 56162419.

[‡] Laboratorio de Fisicoquímica e Ingeniería de Proteínas, Departamento de Bioquímica, Facultad de Medicina.

[§] Departamento de Fisicoquímica, Facultad de Química.

[||] Current address: Institut für Physikalische Chemie der Westfälischen Wilhelms-Universität Münster, Corrensstrasse 30, 48149 Münster, Germany.

[⊥] Current address: Molecular Genetics Unit and CNRS URA2172, Institut Pasteur, 25, rue du Dr. Roux, 75724 Paris, France.

[1] Abbreviations: ANS, 1-anilino-8-naphthalenesulfonate; CD, circular dichroism; DSC, differential scanning calorimetry; DTT, dithiothreitol; EhTIM, triosephosphate isomerase from *Entamoeba histolytica*; FI, fluorescence intensity; Gdn-HCl, guanidine hydrochloride; LmTIM, TIM from *Leishmania mexicana*; mEhTIM, monomeric EhTIM obtained by chemical derivatization; MMTS, methyl methanethiosulfonate; PGA, phosphoglycolic acid; R_s, Stokes radius; ScTIM, TIM from *Saccharomyces cerevisiae*; SCM, spectral center of mass.

10.1021/bi801360k CCC: $40.75
Published on Web 10/07/2008

monomeric intermediates have been reported for TIMs from *Trypanosoma cruzi*, *Trypanosoma brucei*, and *Entamoeba histolytica* (EhTIM) (*8, 9, 18*). All of these conformers are inactive and present decreased secondary structure content. Likewise, pressure studies indicate that the monomeric intermediates of EhTIM and ScTIM are more hydrated than monomeric proteins of a similar size (*18*). Regarding the thermal unfolding of TIM, the presence of hysteresis and some degree of irreversible aggregation are common features. A detailed kinetic characterization of the two-state ScTIM unfolding illustrates that unfolding and refolding rates show large activation enthalpies that may explain the observed hysteresis (*7*). Temperature has been widely used to determine the apparent stability of several wild-type TIMs and their mutants (*6, 7, 19*−*31*). Interestingly, monophasic transitions were obtained in all of these cases. Temperature-induced unfolding intermediates have been observed only for unstable interface mutants (*25*). In this study, we characterized the thermal unfolding of EhTIM and that of a monomeric EhTIM obtained by chemical derivatization of an interface cysteine (mEhTIM) (*32*). We found that the thermal unfolding of EhTIM involves a multistate process with a compact monomeric intermediate. The information obtained from the unfolding of both proteins was used to assign the enthalpic and conformational contributions of dissociation and monomer unfolding.

MATERIALS AND METHODS

α-Glycerol-phosphate dehydrogenase (GDPH) was purchased from Boehringer-Mannheim. All other reagents were purchased from Sigma. All reactants were of analytical grade. The water used was distilled and deionized.

Production, expression, and purification of recombinant wild-type EhTIM were performed as previously described (*20*). Unless otherwise stated, all experiments were carried out in a buffer solution of 20 mM potassium tetraborate and 1 mM dithiothreitol (DTT), pH 8.5 (buffer B).

The derivatization of EhTIM with methyl methanethiosulfonate (MMTS) to obtain a compact monomer (mEhTIM) was done as previously described (*32*). Briefly, EhTIM was incubated in 100 mM triethanolamine, 10 mM EDTA, pH 7.4, and 1.0 mM MMTS at 25 °C for 2 h. Thereafter, the sample was exhaustively dialyzed against 20 mM borate, pH 8.5. All mEhTIM experiments were done in buffer solutions without DTT. Protein concentration was determined using the absorption coefficient calculated from the amino acid sequence $\varepsilon_{280} = 36440\ M^{-1}\ cm^{-1}$ (*20, 33*).

Activity Assays. Catalytic activity was determined by a coupled enzyme assay. One milliliter of reaction cells was prepared in 100 mM triethanolamine, 10 mM EDTA, and 1 mM DTT (pH 8.5) containing 3.0 mM D-glyceraldehyde 3-phosphate, 20 μg of GDPH, and 0.2 mM NADH. Catalytic assays started when 2 ng of EhTIM was added to the reaction cell. Reaction rates were determined following NADH absorbance changes at 340 nm as a function of time in a Beckman DU7500 spectrophotometer at 25 °C (*34*).

Spectroscopic Properties. Circular dichroism (CD) experiments were carried out in a JASCO J-715 spectropolarimeter (Jasco Inc., Easton, MD) equipped with a Pelltier and a water-jacketed cell holder for temperature control. Thermal transitions were followed by continuously monitoring ellipticity changes at 220 nm as a function of temperature (from 25 to 70 °C). Experiments were done in both unfolding and refolding directions. Sample temperature was changed at a constant rate controlled through the Peltier. The heating/cooling rate was 1 °C min^{-1}. EhTIM solutions of 0.1 mg mL^{-1} and 1.0 cm path-length cells were used, and the samples were stirred. CD data corresponding to the first transition were fitted to the Van't Hoff equation.

Fluorescence measurements were made on a PC1 ISS spectrofluorometer (Champaign, IL) equipped with a Peltier and a water-jacketed cell holder for temperature control. TIM concentration was 0.1 mg mL^{-1}, and 1.0 cm cells, which were stirred, were used in all experiments. Thermal transitions were followed by constantly monitoring fluorescence intensity (FI) as a function of temperature. Intrinsic fluorescence measurements were carried out with excitation at 295 nm (2 nm bandwidth) and emission at 333 nm (4 nm bandwidth). Additionally, spectral recordings were made at different temperatures. An automatized protocol was used to obtain fluorescence spectra: samples were excited at 295 nm, and emission spectra (310−410 nm) were taken at every degree change while temperature was ramped from 25 to 90 °C with a 1 °C min^{-1} rate. The fluorescence spectral center of mass (SCM) was calculated from intensity data (I_λ) obtained at different wavelengths: $SCM = \sum \lambda I_\lambda / \sum I_\lambda$. 1-Anilino-8-naphthalenesulfonate (ANS) fluorescence was measured with an excitation wavelength of 360 nm (4 nm bandwidth), and emission was collected in the 400−600 nm range (8 nm bandwidth). Samples (0.1 mg mL^{-1}) were incubated at 20 °C in buffer B with 100 μM ANS for 15 min. Thermal transitions in the presence of the dye were followed using the same automatized protocol described for measuring intrinsic fluorescence spectra.

Calorimetric Experiments. Differential scanning calorimetry (DSC) experiments were done in a VP-DSC calorimeter or in a VP-Capillary DSC system (MicroCal, Northhampton, MA). Measurements were carried out employing heating rates from 0.5 to 2.5 °C min^{-1}. Protein solutions for the calorimetric experiments were prepared by exhaustive dialysis against buffer B, and samples were degassed at room temperature before the calorimetric experiments. In all measurements, buffer from the last dialysis step was used in the reference cell of the calorimeter. In order to ascertain proper equilibration of the instrument, several buffer−buffer baselines were obtained before each run with a protein solution. The last buffer−buffer trace recorded was subtracted from sample endotherms. In some experiments a reheating run was carried out to determine the reversibility of the process. Experiments done with mEhTIM were carried out without DTT. The Origin software package (MicroCal) was used for data analysis, including baseline subtraction and calculation of unfolding enthalpies.

DSC Data Fitting. At high temperature endotherms were distorted by aggregation. Therefore, data fitting was restricted to a limited temperature range, a few degrees above the temperature of the maximum heat capacity of the first transition (*35*). Consequently, experimental data used do not contain information about denaturation heat capacity changes. Endotherms from EhTIM obtained in the 0.2−6.42 mg mL^{-1} range at a scanning rate of 1 °C min^{-1} were fitted to three different dissociation models.

(i) Equilibrium two-state model for dimer dissociation:

$$C_p^{ex} = B_0 + B_1T + \frac{\Delta H}{RT_m^2}\left(\frac{1-f}{-1+\frac{2}{f}}\right) \quad (1)$$

where B_0 and B_1 are the *y*-intercept and the slope of the pretransition, respectively, ΔH is the dissociation enthalpy change, and f is the temperature-dependent fraction of EhTIM molecules in the dimeric state (Microcal Origin 5.0).

(ii) Lumry−Eyring model for dimer dissociation:

$$C_p^{ex} = \frac{\Delta HE_{app}}{RT_m^2}\exp\left(\frac{E_{app}\Delta T}{RT_m^2}\right)\left[1-\frac{1}{2}\exp\left(\frac{E_{app}\Delta T}{RT_m^2}\right)\right] \quad (2)$$

where E_{app} is the apparent activation energy, $\Delta T = T_0 - T_m$, and T_0 is the reference temperature (*36*).

(iii) Takahashi−Sturtevant plot (*37*):

$$\ln C_t = b - \frac{\Delta H}{RT_m} \quad (3)$$

where C_t is the total protein concentration, b is a constant, and T_m is the temperature of the maximum C_p^{ex}. ln C_t vs $1/T_m$ data were fitted to a straight line. ΔH for mEhTIM was obtained from the area endotherms.

Size Exclusion Chromatography. Chromatography experiments were performed at 25 or 42.5 °C on a Superdex 75 HR 10/30 column (Amersham Pharmacia), which was properly thermostated with the use of a circulating water bath that was homemade connected to the column. The column was coupled to an FPLC system (Amersham Pharmacia), equipped with a UV detector (λ = 280 nm) and a Waters 474 fluorescence scanning detector (λ_{exc} = 295 nm; λ_{em} = 333 nm). The column was previously equilibrated with the corresponding buffer before injections. Stokes radii (R_s) were calculated by interpolation from a calibration curve made using eight well-characterized proteins as standards (*38*). Protein concentration (0.1 mg mL^{-1}) was the same as was used in spectroscopic measurements.

Proteolytic Cleavage and NH_2-Terminal Analysis of Electroblotted Fragments. Protein samples were incubated at 1 mg mL^{-1} and 42.5 °C with subtilisin Carlsberg at a 1:2000 (subtilisin:TIM) molar ratio. EhTIM samples with phosphoglycolic acid (PGA), 10 mM, were also incubated at different subtilisin:TIM molar ratios ranging from 1:50 to 1:2000. In all cases proteolysis was arrested by the addition of phenylmethanesulfonyl fluoride (3 mM final concentration). The digested proteins were analyzed via SDS−PAGE at an acrylamide concentration of 16% following the Schägger and von Jagow method (*39*). Gels were stained with Coomassie Brilliant Blue R. Finally, fragments of EhTIM and mEhTIM obtained after 30 min of subtilisin digestion were electroblotted from the gels onto polyvinylidene fluoride membranes (Problott). Semidry transfer was then performed for 2 h at room temperature using as a negative buffer 39.4 mg mL^{-1} aminocaproic acid (pH 8.5) with 0.05% SDS and as a positive buffer 8.2 mg mL^{-1} Tris, 9 mg mL^{-1} Tricine, and 20% methanol. The transferred fragments were stained with Coomassie Brilliant Blue G in 50% methanol. The N-terminal sequence was determined by automated Edman degradation on a gas-phase protein sequencer (LF 3000 Beckman Instruments) equipped with an online Beckman Gold high-performance liquid chromatography (HPLC) system. The HPLC column was a Beckman Spherogel Micro PTH, and the phenylthiohydantoin amino acids were detected using a diode array detector set at 268 and 293 nm for signal and reference, respectively. Each band was submitted to at least 10 Edman degradation cycles. When more than one amino acid was observed, the yield of each identified amino acid was considered for the determination of the sequence of each fragment.

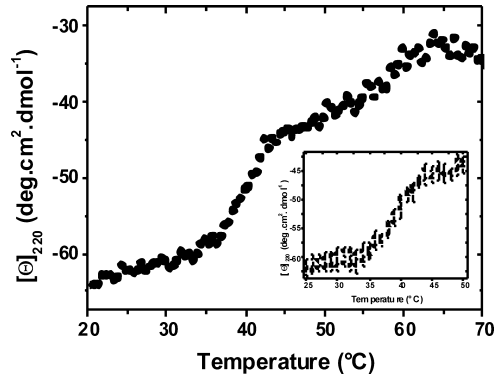

FIGURE 1: Thermal unfolding of EhTIM followed by CD at 220 nm. EhTIM samples (100 μg mL^{-1}) were heated at 1 °C min^{-1}. The inset shows unfolding/refolding data (closed and open symbols, respectively) for the first transition. Refolding data were obtained after heating to 50 °C, with a cooling rate of 1 °C min^{-1}.

Calculations of Accessible Surface Area. Changes in accessible surface area upon dissociation (ΔASA_{Diss}) were calculated for a rigid body dissociation, i.e., as the difference in accessible area between the dimer and the individual monomers; crystallographic coordinates for both were obtained from the PDB file of the native dimer (1M6J). ΔASA for monomer unfolding was estimated by calculating the difference between the isolated monomer and the unfolded state, the latter of which was simulated using the Creamer−Rose method (http://roselab.jhu.edu/utils/unfolded.html) (*40, 41*). Area calculations were performed with the NACCESS program (Simon Hubbard, University College, United Kingdom), an implementation of the Lee and Richards algorithm (*42*), using a probe radius of 1.4 Å and a slab width of 0.05 Å.

The relation between enthalpy changes and apolar and polar ΔASA (ΔASA_{ap} and ΔASA_{pol}, respectively) and/or number of residues (N_{res}) was estimated as follows (*43*):

$$\Delta H(60\ °C) = -8.44\ \text{cal}\ \Delta ASA_{ap}(\text{mol Å}^2)^{-1} + 31.3\ \text{cal}\ \Delta ASA_{pol}(\text{mol Å}^2)^{-1} \quad (4)$$

$$\Delta H(60\ °C) = N_{res}\ 0.69 \pm 0.02\ \text{kcal (mol res)}^{-1} \quad (5)$$

RESULTS

Spectroscopic Characterization of EhTIM Unfolding. Changes in the structural properties of EhTIM induced by temperature were studied using circular dichroism (CD) and intrinsic fluorescence (IF). Thermal unfolding followed by CD showed two transitions indicating the presence of an intermediate (Figure 1). The midpoint of the first transition (T_{m1}) was 41.5 °C, whereas T_{m2} was close to 57 °C. When samples were heated to the end of the second transition (60 °C), protein aggregation was clearly evident. This led to complete irreversibility, as indicated by the lack of recovery of the CD signal when temperature was decreased (data not

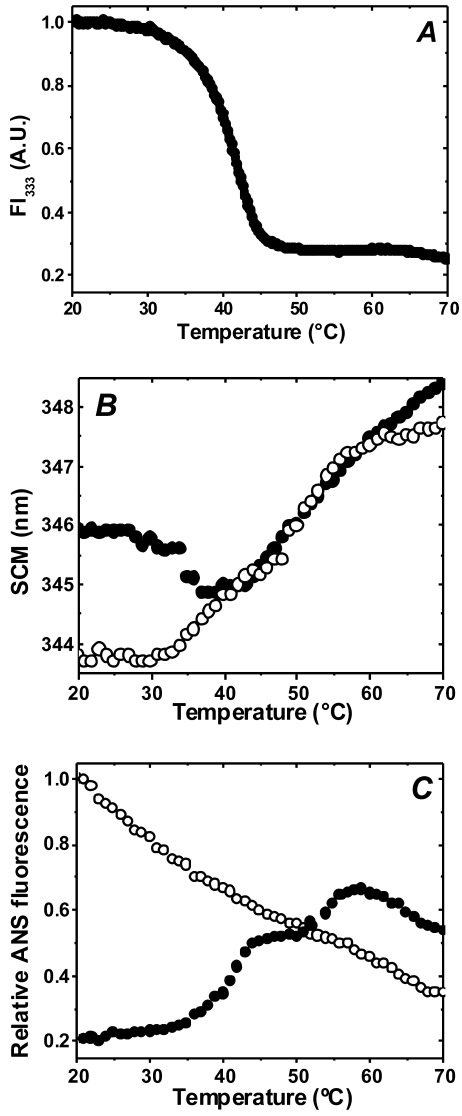

FIGURE 2: Thermal unfolding of EhTIM and mEhTIM followed by fluorescence. Samples (100 μg mL^{-1}) were heated at 1 °C min^{-1}. (A) EhTIM intrinsic fluorescence intensity (λ_{exc} = 295 nm, λ_{em} = 333 nm). (B) SCM of the intrinsic fluorescence spectra of EhTIM (closed symbols) and mEhTIM (open symbols). (C) Normalized ANS fluorescence intensity (λ_{exc} = 360 nm, λ_{em} = 496 nm) (symbols as in panel B).

shown). In contrast, when heating was carried out up to 50 °C, i.e., until the end of the first transition, the CD signal was almost completely recovered after cooling the sample; moreover, the heating/cooling cycle showed almost no hysteresis (Figure 1 inset). Regarding functional properties, about 89% of the original catalytic activity was recovered after a first melt. These results indicate that the first transition is reversible and near equilibrium. Although important changes in secondary structure occurred during the first transition, the intermediate observed at 50 °C retained a significant amount of secondary structure (almost 60% of the native signal at 220 nm).

The temperature-induced unfolding of EhTIM was then followed by fluorescence. The obtained spectra showed changes in both fluorescence intensity (FI) and in spectral center of mass (SCM). In the temperature range that corresponds to the first transition detected by CD, FI showed a marked monophasic decrease (Figure 2A). On the other hand, SCM data showed two transitions (Figure 2B, closed

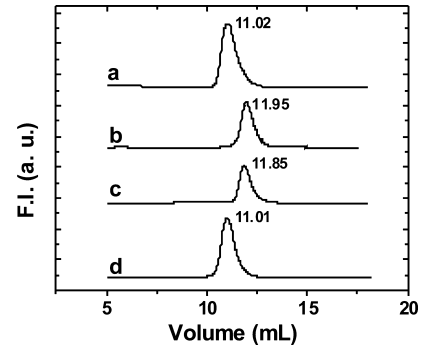

FIGURE 3: Elution profiles of EhTIM and mEhTIM. Proteins (100 μL of 100 μg of TIM mL^{-1}) were injected into a Superdex 75 column, eluted at 1 mL min^{-1}, and detected by fluorescence (λ_{exc} = 295 nm, λ_{em} = 333 nm). Samples and conditions were (a) EhTIM at 25 °C, (b) mEhTIM at 25 °C, (c) EhTIM at 42.5 °C, and (d) EhTIM + 10 mM PGA at 42.5 °C. The numbers over the curves indicate the elution volume of the peak.

symbols). The first one involves a blue shift in SCM (~1 nm), whereas in the second one a red shift occurred, indicating the full exposure of tryptophan residues to the solvent. Thus, the intermediate shows a blue shift in SCM and a decrease in fluorescence intensity when compared with native EhTIM (Figure 2). These fluorescence properties are similar to those reported for a monomeric form of EhTIM (mEhTIM) obtained by chemical derivatization of an interface cysteine by MMTS (*32*). The blue shift in the SCM of mEhTIM has been related to the rearrangement of an interface tryptophan residue (Trp 75) (*32*). The thermal unfolding of mEhTIM and EhTIM (Figure 2B, open and closed symbols, respectively) showed very similar SCM values at temperatures higher than T_{m1}. Therefore, it is likely that the structural rearrangements observed in mEhTIM are similar to those experienced by the EhTIM unfolding intermediate.

To determine the exposure of hydrophobic regions accompanying TIM unfolding, ANS fluorescence was followed as a function of temperature. At 20 °C, ANS binding by mEhTIM is five times higher than that of EhTIM (Figure 2C). This indicates that the derivatized monomer exposes a hydrophobic patch that is not present in the native EhTIM (*32*). However, ANS binding by mEhTIM decreases steadily with temperature, suggesting that monomer unfolding does not involve the exposure of new hydrophobic pockets (Figure 2C, open symbols). ANS binding by EhTIM increased with temperature in a biphasic way with a clear plateau region from 43 to 50 °C. This indicates that the intermediate exposes hydrophobic surface in a way that allows dye binding. At temperatures higher than 55 °C a decrease in ANS binding was observed. It is noted that ANS fluorescence at 70 °C is higher than at 20 °C (Figure 2C, closed symbols). This probably results from aggregation and/or incomplete unfolding of the enzyme.

Association State of the EhTIM Intermediate. The oligomeric state of the EhTIM intermediate was determined by size exclusion chromatography (Figure 3). In accordance to previous reports, at 25 °C the elution profiles of EhTIM and mEhTIM showed single peaks corresponding to Stokes radii (R_s) of 31.2 and 26.3 Å, respectively. The latter is close to the value expected for a compact monomer of the TIM size. The hydrodynamic properties of EhTIM were then determined at an elution-run temperature of 42.5 °C. This

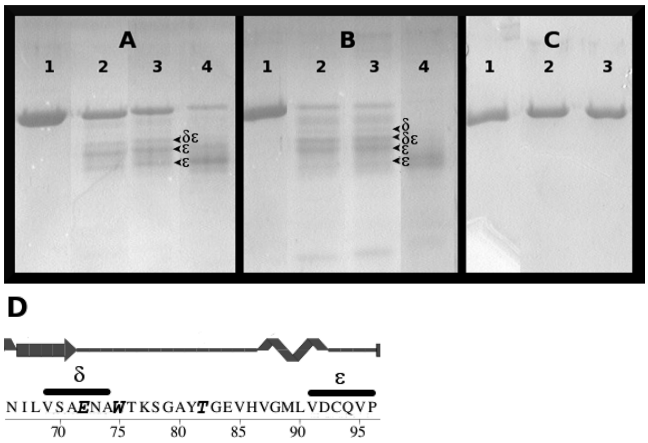

FIGURE 4: Proteolytic cleavage of EhTIM and mEhTIM at 42.5 °C. Time course of EhTIM (panel A) and mEhTIM (panel B) proteolysis by subtilisin (1:2000). Lanes: 1, control; 2, 10 min; 3, 30 min; 4, 45 min. Panel C: Proteolysis of EhTIM samples in the presence of 10 mM PGA. Proteolysis time: 1 h. Lanes: 1, control; 2, EhTIM:subtilisin ratio 1:50; 3, EhTIM:subtilisin ratio 1:200. Panel D shows the amino acid sequence and secondary structure of the β_3/α_3 unit. Solid lines show the amino end sequence of the δ and ε fragments shown in panels A and B.

temperature was chosen because it is close to the end of the first transition and in the upper stability limit of the Superdex resin. A single peak with an R_s of 26.7 Å was observed. The R_s of the intermediate is very similar to the one determined for mEhTIM (Figure 3, compare b and c), indicating that the intermediate observed in the thermal unfolding of EhTIM is a compact monomer. The hydrodynamic properties of EhTIM were then assayed in the presence of phosphoglycolic acid (PGA), a transition state analogue of the substrate (*44*). For this purpose the column was equilibrated and ran at 42.5 °C in buffer containing 10 mM PGA. As expected, ligand binding stabilized the native state, and the elution profile of EhTIM showed the same R_s obtained for the native dimer at 25 °C (Figure 3, compare d and a).

Proteolytic Cleavage. The temperature-induced conformational changes of EhTIM and mEhTIM were also examined by subtilisin proteolytic cleavage. Temporal courses of samples incubated at 42.5 °C with a 1:2000 subtilisin:TIM ratio showed that cleavage was significantly faster for mEhTIM than for EhTIM (Figure 4, compare panels A and B). And yet, a similar fragment distribution was observed in both cases. Moreover, Edman analysis of the proteolytic fragments showed the same two cleavage sites (Val 69 and Val 91) in both proteins (Figure 4D). But when EhTIM was preincubated in the presence of 10 mM PGA, no proteolytic fragments were detected even after a 1 h incubation at a 1:50 subtilisin:TIM ratio (Figure 4C). Figure 3 shows that PGA shifts the elution profile of EhTIM toward the dimeric state, and the absence of proteolysis in the presence of PGA (Figure 4C) showed that the dimer is much less susceptible to subtilisin cleavage than the monomer. This suggests that the observed fragmentation of EhTIM occurs almost exclusively in the monomeric state. Likewise, at 30 °C EhTIM was not digested by subtilisin (data not shown).

Calorimetric Characterization. The thermal stability of EhTIM was then measured by differential scanning calorimetry (DSC). Two endothermic transitions were observed (Figure 6). An exothermic event (irreversible protein aggregation) occurred at the end of the second transition. As expected, aggregation was more evident at high protein concentrations; however, higher heating rates decreased aggregation (data not shown). This suggests that irreversibility is linked to the residence time of EhTIM at high temperatures.

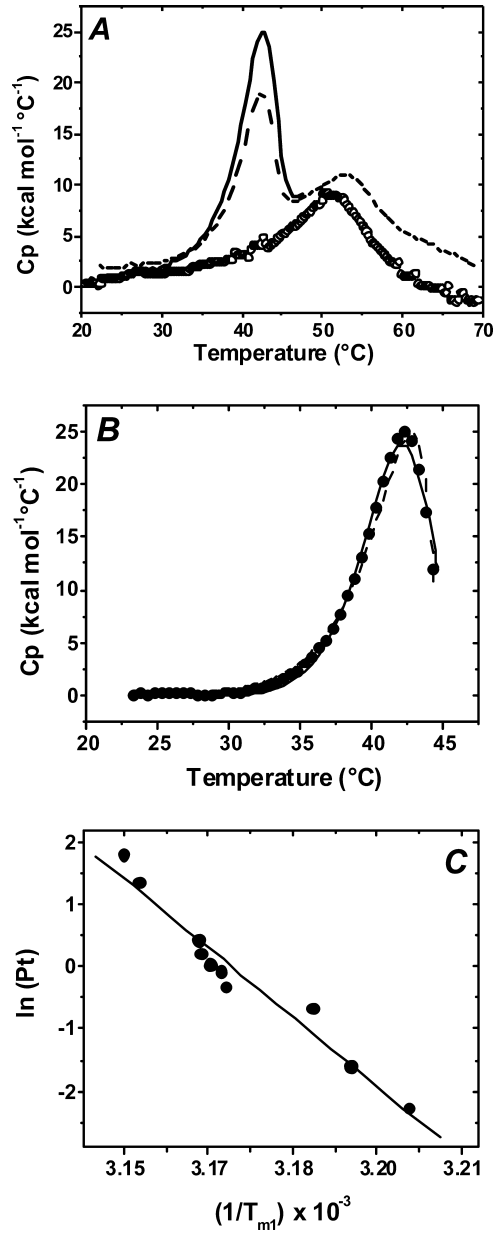

FIGURE 5: Calorimetric analysis of EhTIM and mEhTIM unfolding. (A) DSC profiles of EhTIM and mEhTIM. Samples were heated at a scan rate of 1 °C min^{-1}. EhTIM first scan (solid curve); EhTIM second scan (dashed line); mEhTIM scan (open circles). (B) Representative DSC data fitting for the first transition of EhTIM. Experimental data (closed circles). Area under the curve (ΔH_{Diss} = 133 kcal mol^{-1}). Equilibrium two-state model (eq 1; ΔH_{Diss} = 165 ± 1 kcal mol^{-1}, solid line) and Lumry−Eyring model (eq 2; ΔH_{Diss} = 141 ± 3 kcal mol^{-1}; E_{app} = 70 ± 1 kcal mol^{-1}, dashed line). (C) Takahashi−Sturtevant plot (eq 3; ΔH_{Diss} = 148 ± 20 kcal mol^{-1}, solid line).

Confirming CD melts (Figure 1 inset), considerable reversibility was observed when samples were heated to 50 °C. Under this condition, 70% of the enthalpy change was recovered on a second scan (Figure 5). T_{m1} increased with protein concentration, confirming the bimolecular nature of the first transition. T_{m2} decreased with protein concentration,

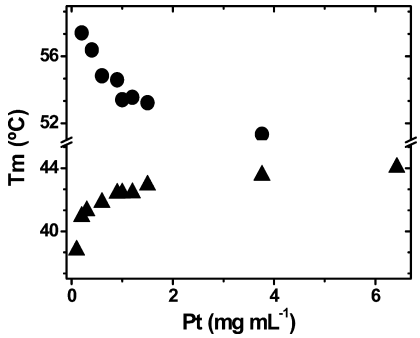

FIGURE 6: Effect of protein concentration on T_m. DSC experiments were done at a scan rate of 1 °C min $^{-1}$. T_{m1} (closed triangles) and T_{m2} (closed circles).

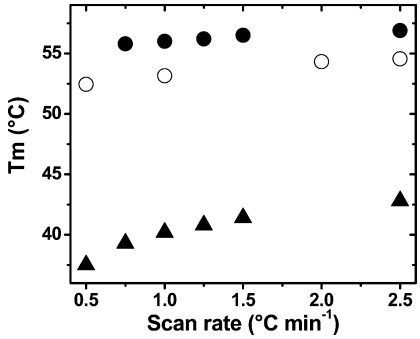

FIGURE 7: Effect of scan rate on T_m. DSC experiments were done at 600 μg mL^{-1}. EhTIM T_{m1} (closed triangles), EhTIM T_{m2} (closed circles), and mEhTIM T_m (open circles).

as expected for a process involving irreversible aggregation (Figure 6). The DSC profile of mEhTIM showed a single irreversible transition with a T_m similar to T_{m2} of EhTIM (Figure 5). This suggests that the unfolding of mEhTIM and that of the monomeric intermediate of EhTIM are similar.

Taken together spectroscopic, hydrodynamic, and calorimetric data clearly indicate that the temperature-induced unfolding of EhTIM involves two steps: reversible subunit dissociation followed by irreversible monomer unfolding.

The enthalpy change for subunit dissociation (ΔH_{Diss}) was calculated by several methods: (i) Van't Hoff analysis: CD data (Figure 1) were analyzed according to a dissociating system. The obtained ΔH_{Diss} value was 140 ± 20 kcal mol^{-1}. DSC experiments carried out in the 0.2−6.42 mg mL^{-1} range were analyzed according to the following four approaches, the reported values of which are the average of ten experiments: (ii) Model-free analysis: The area under DSC curves gave an average calorimetric enthalpy of 137 ± 49 kcal mol^{-1}. (iii) Equilibrium two-state model with dissociation: DSC data fitted to this model (see eq 1) gave an average ΔH_{Diss} = 163 ± 19 kcal mol^{-1}. (iv) Lumry−Eyring model: DSC runs carried out at different scan rates showed a slight increase in the T_m values of EhTIM and mEhTIM (Figure 7). Therefore, DSC profiles were also fitted to a kinetic model that includes irreversible aggregation (eq 2). This gives ΔH_{Diss} = 146 ± 53 kcal mol^{-1} and an activation energy (E_{app}) = 66.2 ± 7 kcal mol^{-1}. (v) Takahashi−Sturtevant plot (*37*): The enthalpy change calculated from a plot of the $1/T_m$ vs natural logarithm of protein concentration (Figure 5C) gives ΔH_{Diss} = 148 ± 20 kcal mol^{-1}. The fittings for approaches iii and iv are very similar (Figure 5B). The average obtained from all of these approaches (i−iv) gives ΔH_{Diss} = 146.8 ± 10 kcal mol^{-1}.

The estimation of the enthalpy change for monomer unfolding (ΔH_{Unf}) from the second calorimetric transition of EhTIM is complicated because the pre- and posttransition baselines are contaminated by dimer dissociation and monomer aggregation, respectively. Therefore, as a first approximation, we have used the mEhTIM endotherm for the estimation of ΔH_{Unf}. This choice is based on the fact that the secondary structure content, hydrodynamic properties, SCM unfolding profiles, and T_m of mEhTIM are similar to those of the monomeric intermediate of EhTIM, and ΔH_{Unf} calculated from the area under the DSC endotherms of mEhTIM gives 59.6 ± 4.5 kcal mol $^{-1}$.

DISCUSSION

Monomeric intermediates have been frequently observed in both kinetic and equilibrium studies on TIM unfolding induced by urea or Gdn-HCl (*8−10, 12−14, 18, 45*). In contrast, thermal unfolding studies show monophasic transitions (*6, 7, 19−30*). This is the first report on the characterization of a monomeric intermediate in the thermal unfolding of a TIM. An unusual property of the EhTIM interface is the presence of glutamine at position 72, while the equivalent position in almost all TIMs is a glutamate residue. This characteristic is shared between EhTIM and the TIM from *Leismania mexicana* (LmTIM). It has been shown that the ionization of this residue destabilizes LmTIM and causes a pH-dependent unfolding profile (*6, 19*). The stability of EhTIM also seems to be pH-dependent: At pH 7.4 a monophasic transition with a T_m near 60 °C was observed (*20*), whereas in the present work at pH 8.5 two transitions with lower T_m values were observed.

Spectroscopic, calorimetric, and chromatographic techniques showed that the temperature-induced unfolding of EhTIM is a multistate process with at least two transitions. The first step involves the reversible dissociation of the native state into a monomeric intermediate, while the second one is related to monomer unfolding and linked to irreversible protein aggregation. The monomeric intermediate is inactive and compact (R_s native = 31.2 Å, R_s intermediate = 26.7 Å), and it has residual secondary structure (~60% of the CD signal at 222 nm), decreased fluorescence intensity, and a 1 nm blue shift in the SCM. Both the monomeric intermediate and mEhTIM are compact. In contrast, all of the monomeric intermediates thus far reported are expanded.

The different approaches employed in this work to calculate ΔH_{Diss} gave similar values, indicating that the average ΔH_{Diss} (146.8 ± 10 kcal mol^{-1}) is a good estimation. Regarding monomer unfolding, the enthalpy change estimated from mEhTIM data is ΔH_{Unf} = 59.6 ± 4.5 kcal mol $^{-1}$. The total enthalpy change (ΔH_{Tot}) for the dissociation and unfolding of EhTIM ($\Delta H_{Tot} = \Delta H_{Diss} + 2\Delta H_{Unf}$) is 266 kcal mol^{-1}. This value is in the range of that obtained for the thermal unfolding of ScTIM (250−318 kcal mol^{-1}) (*7*).

The ΔH_{Diss} value calculated for the rigid body dissociation of TIM monomers (see Materials and Methods), i.e., the exposure of the 74 interface residues (37 per monomer), is between 11 and 51 kcal mol^{-1} (based on the ΔASA or on the number of exposed residues, respectively). Thus, the experimental ΔH_{Diss} is much higher than the theoretical estimate. In contrast, the experimental ΔH_{Unf} is 59.6 ± 4.5 kcal mol^{-1}, much lower than the estimated ΔH_{Unf} for the

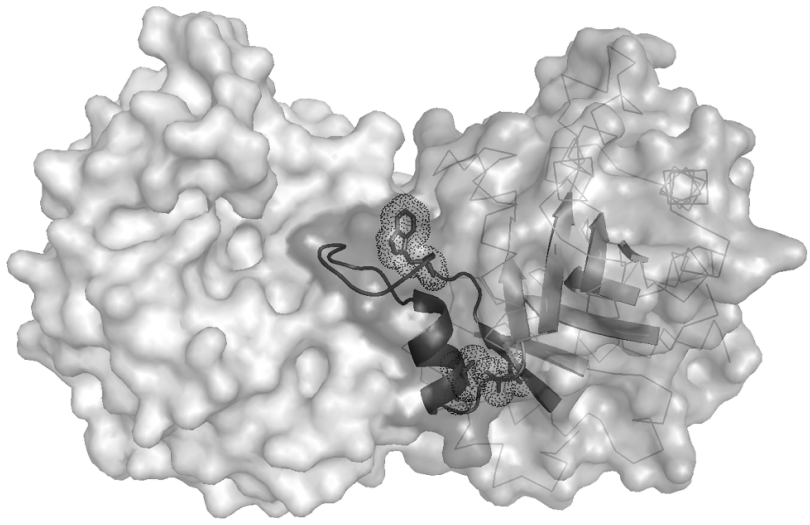

FIGURE 8: The structure of EhTIM. The surface of the two monomers is presented in different shades. For subunit A, the C_α trace is shown in lines, the β barrel is depicted in cartoons, the β_3/α_3 unit (Figure 4D) is shown as dark cartoons, and Trp 75, Val 69, and Val 91 are shown as sticks with van der Waals surface in dots. This figure was generated with Pymol (*49*) using pdb file 1m6j.

unfolding of the 261 aa of each monomer (110 or 180 kcal mol^{-1}, based on the ΔASA or on the number of residues, respectively).

The total ΔH estimated for the dissociation and unfolding of EhTIM is 220−360 kcal mol^{-1}. The experimental value $\Delta H_{Tot} = 266$ kcal mol^{-1} is in this range. It is noteworthy that the experimental ΔH_{Diss} is higher and the experimental ΔH_{Unf} is lower than the values expected for the rigid body dissociation of the dimer followed by the unfolding of native-like monomers. This indicates that dissociation involves not only the hydration of the interface but also the unfolding of other regions. According to enthalpy parametrizations, the experimental ΔH_{Diss} corresponds to the unfolding of ∼106 residues per monomer, since the interface of EhTIM is composed of ∼37 residues, suggesting that in each subunit approximately 69 additional residues become solvated upon dissociation. Experimental evidence that extensive unfolding occurs with dissociation comes from the exposure of hydrophobic patches in the monomeric intermediate, as deduced from the increased ANS binding upon dissociation. Similarly, ΔV_{Unf} for the pressure unfolding of the EhTIM monomeric intermediate indicates that this conformer is more hydrated than folded monomers of similar size (*18*). Fluorescence experiments indicate that, as a consequence of dissociation, structural rearrangements take place in the neighborhood of Trp 75 located in loop 3. This conformational change is expected since loop 3 is the main interface loop. It should be noted that monomerization also involves structural rearrangements in regions that are not part of the interface. For example, Val 69 and Val 91, located in β_3 and α_3, respectively, are accessible to subtilisin in the monomer but not in the dimer (Figure 8). This suggests that the whole β_3/α_3 unit (Figures 4D and 8) is completely rearranged in the monomeric intermediate. This motif contributes to nearly one-third of the interface residues. Besides its structural role, residues located in loop 3 such as Thr 82 have been implicated in the proper alignment of catalytic residues (*29*).

The experimental results presented in this work indicate that before association TIM monomers are only partially folded. A similar behavior was observed in simulations using a minimalist Go model (*46*). The partially structured nature of the intermediate should increase both flexibility and the capture radius, thereby enhancing the speed of association. This behavior has been termed the "fly-casting mechanism" (*47*). In this regard, we have previously shown that TIM association is a very efficient process, limited only by monomer diffusion through the solvent (*48*). The coupling between folding and association suggests that the interface plays a central role on the stability and function of TIM. Studies with mutants obtained by *in silico* design and directed evolution have shown that changes at the interface affect not only the assembly and stability of the protein but also its catalytic properties (*25*). The significant gain of structure upon association places the interface as a final nucleation motif that directs/controls both the global folding of the protein and the construction of the active site geometry.

ACKNOWLEDGMENT

We thank Prof. M. Costas and Prof. J. M. Sánchez-Ruiz for helpful suggestions and for the use of the DSC calorimeters at the UNAM and the Universidad de Granada, respectively, Dr. H. Reyes-Vivas and M. Sc. I. De la Mora-De la Mora for help, advice, and suggestions in proteolysis experiments, and Mns. Lenin Domínguez-Ramírez and Nacha Cattan for valuable suggestions and unselfish involvement.

REFERENCES

1. Banner, D. W., Bloomer, A. C., Petsko, G. A., Phillips, D. C., Pogson, C. I., Wilson, I. A., Corran, P. H., Furth, A. J., Milman, J. D., Offord, R. E., Priddle, J. D., and Waley, S. G. (1975) Structure of chicken muscle triose phosphate isomerase determined crystallographically at 2.5 angstrom resolution using amino acid sequence data. *Nature 255*, 609–614.
2. Wierenga, R. K., Noble, M. E., and Davenport, R. C. (1992) Comparison of the refined crystal structures of liganded and unliganded chicken, yeast and trypanosomal triosephosphate isomerase. *J. Mol. Biol. 224*, 1115–1126.
3. Maes, D., Zeelen, J. P., Thanki, N., Beaucamp, N., Alvarez, M., Thi, M. H., Backmann, J., Martial, J. A., Wyns, L., Jaenicke, R., and Wierenga, R. K. (1999) The crystal structure of triosephosphate isomerase (TIM) from Thermotoga maritima: a comparative

thermostability structural analysis of ten different TIM structures. *Proteins: Struct., Funct., Genet. 37*, 441–453.
4. Mainfroid, V., Terpstra, P., Beauregard, M., Frere, J. M., Mande, S. C., Hol, W. G., Martial, J. A., and Goraj, K. (1996) Three hTIM mutants that provide new insights on why TIM is a dimer. *J. Mol. Biol. 257*, 441–456.
5. Rietveld, A. W., and Ferreira, S. T. (1998) Kinetics and energetics of subunit dissociation/unfolding of TIM: the importance of oligomerization for conformational persistence and chemical stability of proteins. *Biochemistry 37*, 933–937.
6. Lambeir, A. M., Backmann, J., Ruiz-Sanz, J., Filimonov, V., Nielsen, J. E., Kursula, I., Norledge, B. V., and Wierenga, R. K. (2000) The ionization of a buried glutamic acid is thermodynamically linked to the stability of Leishmania mexicana triose phosphate isomerase. *Eur. J. Biochem. 267*, 2516–2524.
7. Benitez-Cardoza, C. G., Rojo-Dominguez, A., and Hernandez-Arana, A. (2001) Temperature-induced denaturation and renaturation of triosephosphate isomerase from Saccharomyces cerevisiae: evidence of dimerization coupled to refolding of the thermally unfolded protein. *Biochemistry 40*, 9049–9058.
8. Chanez-Cardenas, M. E., Fernandez-Velasco, D. A., Vazquez-Contreras, E., Coria, R., Saab-Rincon, G., and Perez-Montfort, R. (2002) Unfolding of triosephosphate isomerase from Trypanosoma brucei: identification of intermediates and insight into the denaturation pathway using tryptophan mutants. *Arch. Biochem. Biophys. 399*, 117–129.
9. Chanez-Cardenas, M. E., Perez-Hernandez, G., Sanchez-Rebollar, B. G., Costas, M., and Vazquez-Contreras, E. (2005) Reversible equilibrium unfolding of triosephosphate isomerase from Trypanosoma cruzi in guanidinium hydrochloride involves stable dimeric and monomeric intermediates. *Biochemistry 44*, 10883–10892.
10. Najera, H., Costas, M., and Fernandez-Velasco, D. A. (2003) Thermodynamic characterization of yeast triosephosphate isomerase refolding: insights into the interplay between function and stability as reasons for the oligomeric nature of the enzyme. *Biochem. J. 370*, 785–792.
11. Zomosa-Signoret, V., Hernandez-Alcantara, G., Reyes-Vivas, H., Martinez-Martinez, E., Garza-Ramos, G., Perez-Montfort, R., Tuena De Gomez-Puyou, M., and Gomez-Puyou, A. (2003) Control of the reactivation kinetics of homodimeric triosephosphate isomerase from unfolded monomers. *Biochemistry 42*, 3311–3318.
12. Morgan, C. J., Wilkins, D. K., Smith, L. J., Kawata, Y., and Dobson, C. M. (2000) A compact monomeric intermediate identified by NMR in the denaturation of dimeric triose phosphate isomerase. *J. Mol. Biol. 300*, 11–16.
13. Zabori, S., Rudolph, R., and Jaenicke, R. (1980) Folding and association of triose phosphate isomerase from rabbit muscle. *Z. Naturforsch. C35*, 999–1004.
14. Waley, S. G. (1973) Refolding of triose phosphate isomerase. *Biochem. J. 135*, 165–172.
15. Garza-Ramos, G., Tuena de Gomez-Puyou, M., Gomez-Puyou, A., and Gracy, R. W. (1992) Dimerization and reactivation of triosephosphate isomerase in reverse micelles. *Eur. J. Biochem. 208*, 389–395.
16. Silverman, J. A., and Harbury, P. B. (2002) The equilibrium unfolding pathway of a $(\beta/\alpha)_8$ barrel. *J. Mol. Biol. 324*, 1031–1040.
17. Pan, H., Raza, A. S., and Smith, D. L. (2004) Equilibrium and kinetic folding of rabbit muscle triosephosphate isomerase by hydrogen exchange mass spectrometry. *J. Mol. Biol. 336*, 1251–1263.
18. Vazquez-Perez, A. R., and Fernandez-Velasco, D. A. (2007) Pressure and denaturants in the unfolding of triosephosphate isomerase: the monomeric intermediates of the enzymes from Saccharomyces cerevisiae and Entamoeba histolytica. *Biochemistry 46*, 8624–8633.
19. Williams, J. C., Zeelen, J. P., Neubauer, G., Vriend, G., Backmann, J., Michels, P. A., Lambeir, A. M., and Wierenga, R. K. (1999) Structural and mutagenesis studies of leishmania triosephosphate isomerase: a point mutation can convert a mesophilic enzyme into a superstable enzyme without losing catalytic power. *Protein Eng. 12*, 243–250.
20. Landa, A., Rojo-Dominguez, A., Jimenez, L., and Fernandez-Velasco, D. A. (1997) Sequencing, expression and properties of triosephosphate isomerase from Entamoeba histolytica. *Eur. J. Biochem. 247*, 348–355.
21. Hernandez-Alcantara, G., Garza-Ramos, G., Hernandez, G. M., Gomez-Puyou, A., and Perez-Montfort, R. (2002) Catalysis and stability of triosephosphate isomerase from Trypanosoma brucei with different residues at position 14 of the dimer interface. Characterization of a catalytically competent monomeric enzyme. *Biochemistry 41*, 4230–4238.
22. Gopal, B., Ray, S. S., Gokhale, R. S., Balaram, H., Murthy, M. R., and Balaram, P. (1999) Cavity-creating mutation at the dimer interface of Plasmodium falciparum triosephosphate isomerase: restoration of stability by disulfide cross-linking of subunits. *Biochemistry 38*, 478–486.
23. Mixcoha-Hernandez, E., Moreno-Vargas, L. M., Rojo-Dominguez, A., and Benitez-Cardoza, C. G. (2007) Thermal-unfolding reaction of triosephosphate isomerase from Trypanosoma cruzi. *Protein J. 26*, 491–498.
24. Gonzalez-Mondragon, E., Zubillaga, R. A., Saavedra, E., Chanez-Cardenas, M. E., Perez-Montfort, R., and Hernandez-Arana, A. (2004) Conserved cysteine 126 in triosephosphate isomerase is required not for enzymatic activity but for proper folding and stability. *Biochemistry 43*, 3255–3263.
25. Peimbert, M., Dominguez-Ramirez, L., and Fernandez-Velasco, D. A. (2008) Hydrophobic repacking of the dimer interface of triosephosphate isomerase by in silico design and directed evolution. *Biochemistry 47*, 5556–5564.
26. Reyes-Lopez, C. A., Gonzalez-Mondragon, E., Benitez-Cardoza, C. G., Chanez-Cardenas, M. E., Cabrera, N., Perez-Montfort, R., and Hernandez-Arana, A. (2008) The conserved salt bridge linking two C-terminal β/α units in homodimeric triosephosphate isomerase determines the folding rate of the monomer. *Proteins: Struct., Funct., Genet. 72*, 972–979.
27. Cabrera, N., Hernandez, A., Gloria, Mendoza, H., Guillermo, Gomez-Puyou, A., and Perez-Montfort, R. (2008) Key residues of loop 3 in the interaction with the interface residue at position 14 in triosephosphate isomerase from Trypanosoma brucei. *Biochemistry 47*, 3499–3506.
28. Schliebs, W., Thanki, N., Eritja, R., and Wierenga, R. (1996) Active site properties of monomeric triosephosphate isomerase (monoTIM) as deduced from mutational and structural studies. *Protein Sci. 5*, 229–239.
29. Schliebs, W., Thanki, N., Jaenicke, R., and Wierenga, R. K. (1997) A double mutation at the tip of the dimer interface loop of triosephosphate isomerase generates active monomers with reduced stability. *Biochemistry 36*, 9655–9662.
30. Sun, J., and Sampson, N. S. (1999) Understanding protein lids: kinetic analysis of active hinge mutants in triosephosphate isomerase. *Biochemistry 38*, 11474–11481.
31. Cabrera, N., Hernandez-Alcantara, G., Mendoza-Hernandez, G., Gomez-Puyou, A., and Perez-Montfort, R. (2008) Key residues of loop 3 in the interaction with the interface residue at position 14 in triosephosphate isomerase from Trypanosoma brucei. *Biochemistry 47*, 3499–3506.
32. Rodriguez-Romero, A., Hernandez-Santoyo, A., del Pozo Yauner, L., Kornhauser, A., and Fernandez-Velasco, D. A. (2002) Structure and inactivation of triosephosphate isomerase from Entamoeba histolytica. *J. Mol. Biol. 322*, 669–675.
33. Pace, C. N., Vajdos, F., Fee, L., Grimsley, G., and Gray, T. (1995) How to measure and predict the molar absorption coefficient of a protein. *Protein Sci. 4*, 2411–2423.
34. Rozacky, E. E., Sawyer, T. H., Barton, R. A., and Gracy, R. W. (1971) Studies on human triosephosphate isomerase. I. Isolation and properties of the enzyme from erythrocytes. *Arch. Biochem. Biophys. 146*, 312–320.
35. Thorolfsson, M., Ibarra-Molero, B., Fojan, P., Petersen, S. B., Sanchez-Ruiz, J. M., and Martinez, A. (2002) L-phenylalanine binding and domain organization in human phenylalanine hydroxylase: a differential scanning calorimetry study. *Biochemistry 41*, 7573–7585.
36. Sanchez-Ruiz, J. M. (1992) Theoretical analysis of Lumry-Eyring models in differential scanning calorimetry. *Biophys. J. 61*, 921–935.
37. Takahashi, K., and Sturtevant, J. M. (1981) Thermal denaturation of streptomyces subtilisin inhibitor, subtilisin BPN′, and the inhibitor-subtilisin complex. *Biochemistry 20*, 6185–6190.
38. Uversky, V. N. (1993) Use of fast protein size-exclusion liquid chromatography to study the unfolding of proteins which denature through the molten globule. *Biochemistry 32*, 13288–13298.
39. Schägger, H., and von Jagow, G. (1987) Tricine-sodium dodecyl sulfate polyacrylamide gel electrophoresis for the separation of proteins in the range of 1 to 100 kDa. *Anal. Biochem. 166*, 368–379.

40. Creamer, T. P., Srinivasan, R., and Rose, G. D. (1995) Modeling unfolded states of peptides and proteins. *Biochemistry 34*, 16245–16250.
41. Creamer, T. P., Srinivasan, R., and Rose, G. D. (1997) Modeling unfolded states of proteins and peptides. II. Backbone solvent accessibility. *Biochemistry 36*, 2832–2835.
42. Lee, B., and Richards, F. M. (1971) The interpretation of protein structures: estimation of static accessibility. *J. Mol. Biol. 55*, 379–400.
43. Xie, D., and Freire, E. (1994) Molecular basis of cooperativity in protein folding. V. Thermodynamic and structural conditions for the stabilization of compact denatured states. *Proteins: Struct., Funct., Genet. 19*, 291–301.
44. Wolfenden, R. (1969) Transition state analogues for enzyme catalysis. *Nature 223*, 704–705.
45. Vázquez-Contreras, E., Zubillaga, R., Mendoza-Hernández, G., Costas, M., and Fernández-Velasco, D. A. (2000) Equilibrium unfolding of yeast triosephosphate isomerase: A monomeric intermediate in guanidine-HCl and two-state behavior in urea. *Protein Pept. Lett. 7*, 57–64.
46. Patel, B., and Finke, J. M. (2007) Folding and unfolding of gammaTIM monomers and dimers. *Biophys. J. 93*, 2457–2471.
47. Levy, Y., Cho, S. S., Onuchic, J. N., and Wolynes, P. G. (2005) A survey of flexible protein binding mechanisms and their transition states using native topology based energy landscapes. *J. Mol. Biol. 346*, 1121–1145.
48. Najera, H., Dagdug, L., and Fernandez-Velasco, D. A. (2007) Thermodynamic and kinetic characterization of the association of triosephosphate isomerase: the role of diffusion. *Biochim. Biophys. Acta 1774*, 985–994.
49. DeLano, W. L. (2002)The Pymol Molecular Graphics System, DeLano Scientific, San Carlos, CA.

BI801360K